Electrostatic force microscopy: imaging DNA and protein polarizations one by one

2009 Nanotechnology 20 145102

(http://iopscience.iop.org/0957-4484/20/14/145102)

Nanotechnology **20** (2009) 145102 (6pp) doi:10.1088/0957-4484/20/14/145102

Electrostatic force microscopy: imaging DNA and protein polarizations one by one

Eriko Mikamo-Satoh[1,2], **Fumihiko Yamada**[1], **Akihiko Takagi**[1], **Takuya Matsumoto**[1,3] **and Tomoji Kawai**[1,3]

[1] Institute of Scientific and Industrial Research, Osaka University, 8-1 Mihogaoka, Ibaraki, Osaka 567-0047, Japan
[2] Department of Pharmacy, Hyogo University of Health Sciences, 1-3-6 Minatojima, Chuo-ku, Kobe, Hyogo 650-8530, Japan

E-mail: matsumoto@sanken.osaka-u.ac.jp and kawai@sanken.osaka-u.ac.jp

Received 24 October 2008, in final form 5 December 2008
Published 17 March 2009
Online at stacks.iop.org/Nano/20/145102

Abstract
We present electrostatic force microscopy images of double-stranded DNA and transcription complex on an insulating mica substrate obtained with molecular resolution using a frequency-mode noncontact atomic force microscope. The electrostatic potential images show that both DNA and transcription complexes are polarized with an upward dipole moment. Potential differences of these molecules from the mica substrate enabled us to estimate dipole moments of isolated DNA and transcription complex in zero external field to be 0.027 D/base and 0.16 D/molecule, respectively. Scanning capacitance microscopy demonstrates characteristic contrast inversion between DNA and transcription complex images, indicating the difference in electric polarizability of these molecules. These findings indicate that the electrostatic properties of individual biological molecules can be imaged on an insulator substrate while retaining complex formation.

S Supplementary data are available from stacks.iop.org/Nano/20/145102

1. Introduction

Visualization of biomolecules is one of the main aspects of modern molecular biology. In many cases, biomolecules are labeled with a fluorescent molecule and the fluorescence of the resulting conjugate is probed using fluorescent microscopy. In this method, observed images give only the trace of biomolecules, and the behavior of biomolecules is deduced from these images. Atomic force microscopy (AFM) holds a unique position for bioimaging at the single-molecule level because this method can provide direct information regarding the structure and properties of biomolecules without labeling or staining. For example, AFM studies have revealed structures of string-like DNA and RNA [1–5], globular proteins [6] and ribosomes [7], as well as various types of cells [8, 9] and the mechanical properties of membranes [10]. These achievements indicate that AFM is clearly beneficial and a powerful methodology for molecular biology.

Here, we report polarization imaging of biomolecules on an insulator substrate by electrostatic force microscopy (EFM) based on frequency-mode noncontact AFM. Polarization of biomolecules is a key issue in biomolecular recognition. However, no effective experimental method has been developed to observe the polarization of biomolecules at the molecular scale. This difficulty arises from the limitation that Kelvin probe force microscopy, which is the conventional method for such polarization observations, requires a metal substrate applying a well-defined electric field to the target molecules [11]. This requirement results in inactivation of biomolecules and conflicts with the requirement for insulating substrates, such as mica, to be used to support biomolecules on surfaces while retaining the biomolecular functions. Recently, this problem was resolved by our finding that the polarization of molecules could be imaged even on thick (millimeter-scale) insulating substrates using an inhomogeneous electric field around a sharp tip apex and highly sensitive electrostatic force detection by frequency-mode noncontact AFM.

In this paper, we describe the electrostatic potential and capacitance measurements of DNA and transcription complex on a mica substrate. The measurements provided clear images reflecting the polarization of these molecules.

[3] Authors to whom any correspondence should be addressed.

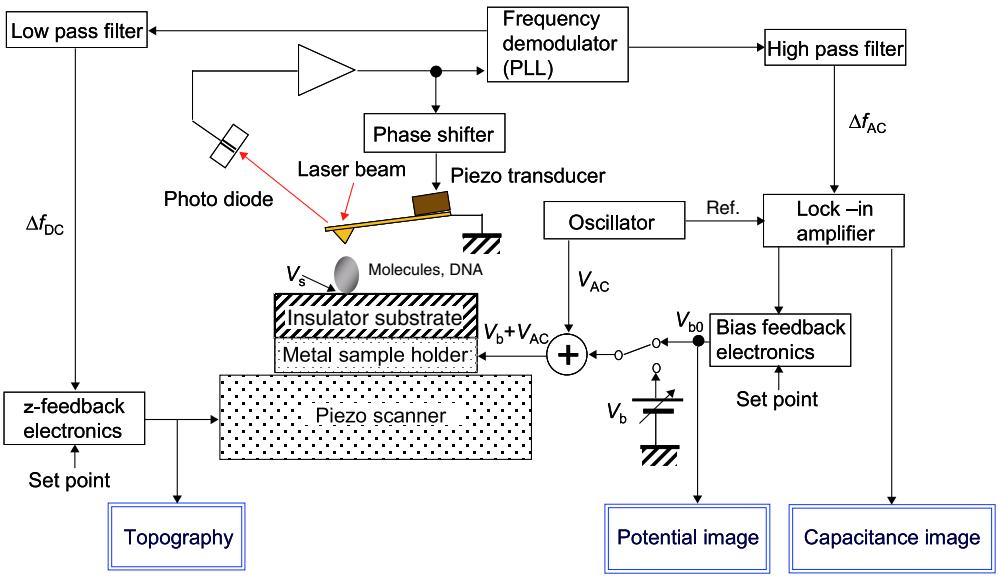

Figure 1. Schematic diagram of apparatus.
(This figure is in colour only in the electronic version)

These results show that DNA on a mica substrate has an electric dipole induced by adsorption, and the positive part of RNA polymerase binds to DNA in a transcription complex. Furthermore, capacitance images give contrast inversion between DNA and transcription complex. These phenomena are potentially useful for the distinction of RNA polymerase from particle-like structures of tangled DNA, which are often confused with proteins on AFM observation.

2. Experimental details

2.1. Preparation of DNA and protein complex

An *in vitro* transcription system used for electrostatic force microscopy measurement was prepared by mixing 20 U of T7 phage-derived RNA polymerase, 500 ng of circular plasmid DNA and a mixture of three nucleotides (ATP, UTP and GTP, 0.25 mM each) in 50 μl of transcription buffer A (20 mM Tris-HCl, pH 8.0, 6 mM $MgCl_2$, 5 mM DTT and 1 mM spermidine). The plasmid DNA is commercially available as pIVEX control vector GFP (Roche), which contains T7 promoter sequence. T7 RNA polymerase recognizes the sequence to start the transcription. Transcription was carried out at 37 °C for 10 min, and the reaction mixture was immediately purified using a YM-100 spin column (Millipore) by size exclusion in accordance with the manufacturer's instructions. The purified solution was deposited on the freshly cleaved mica substrate (Nilaco), and left for 3 min at room temperature. The mica surface was then rinsed with 1 ml of sterile RNase-free water, and dried. The sample was mounted on a gold sample holder with argental paste for electrostatic force microscopy measurement.

2.2. Electrostatic force microscopy measurement

A schematic diagram of the apparatus for EFM measurements is shown in figure 1. The experiments were performed using a modified scanning probe microscope (JSPM-4200; JEOL) at a pressure of 10^{-4} mbar with Ti/Pt-coated cantilevers (spring constant = 14 N m^{-1}, resonance frequency = 315 kHz). To avoid unexpected charge injection from the tip to the sample surface, the topography and electrostatic images were taken in noncontact mode with frequency-shift detection using a frequency demodulator (EasyPLL; Nanosurf). In this mode, the cantilever oscillation is self-excited at the resonance frequency, and the frequency shift Δf is proportional to $\partial F/\partial z$, where F means the electrostatic force between the tip and the sample with their separation z [12]. The backside bias voltage V_b is applied to the sample holder in close contact with the backside of the substrate, as shown in figure 2(a). AC modulation at a frequency of 1 kHz and amplitude of 1 V is superposed on V_b for lock-in detection. The V_b generates the externally-applied surface potential V_s.

Generally, electrostatic force shows quadratic dependence on the potential difference between the tip and the substrate surface. The applied surface potential V_{s0} can be found for the minimal force (figure 2(b) upper). For an insulator substrate, the V_{s0} value is affected by surface charge and electric dipoles of adsorbed molecules. Usually, the adsorbed molecules contribute to local variation of surface potential. Accordingly, simultaneous observation of topography and electrostatic potential image can discriminate the molecular dipoles from the electrification at the insulating substrate surface indicating broad potential variation.

During topographic image acquisition, the V_{b0} values providing V_{s0} are determined at every pixel by feedback control with lock-in output of the AC component at zero. For this purpose, surface potential modulation by an external bias voltage is essential to obtain an electrical potential image by feedback operation using lock-in detection. The spatial variation of V_{b0} reflects that of V_{s0} at the substrate surface,

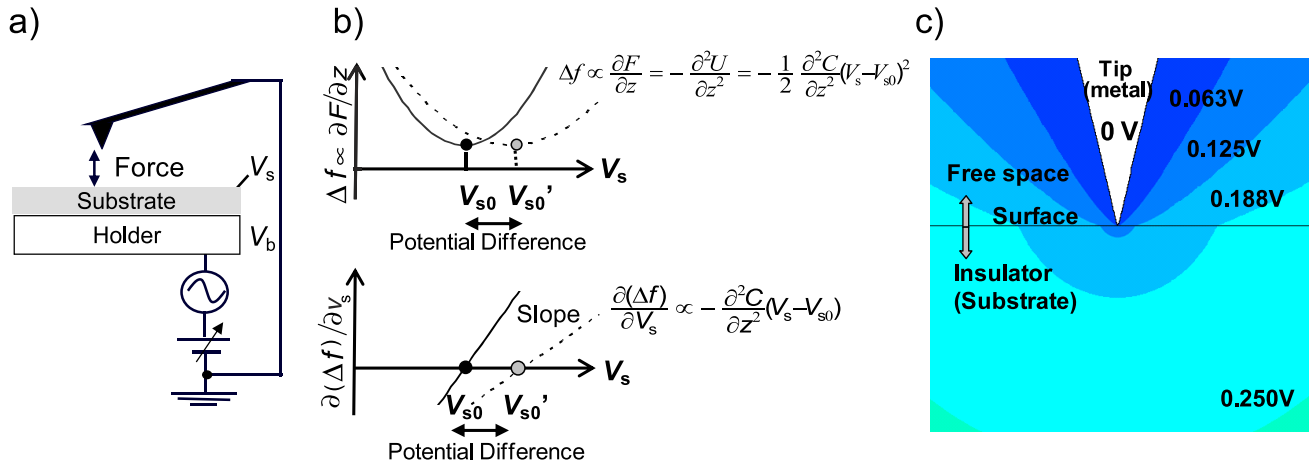

Figure 2. Principle of electrostatic force microscopy. (a) Schematic illustration of electrostatic force microscopy measurement. Bias voltage V_b is applied between the tip and the electrode closely contacting with the backside of the substrate. The substrate is an insulator and its surface is not biased directly. Electrostatic force is determined by the potential difference between the tip (grounded) and substrate surface V_s. AC modulation is superposed on DC bias for lock-in amplifier detection. (b) Schematic representation of the electrostatic force between the tip and sample F as a function of the electric potential at the sample surface V_s (upper). The curve is parabolic and the minimal voltages V_{s0} compensate for the surface electric potential. The surface potential difference indicates the variation of electric potential induced by adsorbates. Schematic plot of capacitance $\partial(\Delta f)/\partial V_s$ versus V_s (lower). The slopes reflect the dielectric constant of adsorbate and variations of X-axis intersection indicate surface potential differences. (c) Potential map calculated by finite element calculation assuming that the tip radius is 20 nm, tip–sample separation is 5 nm, insulating substrate thickness is 1 mm and substrate dielectric constant is 6. Backside bias voltage is 1 V and the tip is grounded.

including adsorbate effects. However, the images taken by V_{b0} mapping do not indicate absolute values of surface potential distribution directly because the bias voltage is applied to the sample holder in contact with the backside of the insulator substrate. In the case that the distance from the surface to some grounded object is far larger than the substrate thickness, the V_s is almost the same as the V_b. In contrast, assuming the parallel plate electrodes, the V_s at the surface below the tip is almost zero due to the nanoscale tip–sample separation, which is far smaller than the substrate thickness. However, in consideration of an actual acuminate tip, the shape effect is essential to the electric potential imaging at the surface of insulating materials. The electric field can penetrate into the insulating material and the V_s just below the tip is large enough to modulate the surface potential. Assuming 20 nm of tip radius, 5 nm of tip–sample distance, and 1 mm of substrate thickness, the finite element calculation shows that the V_s is a tenth of V_b, as shown in figure 2(c), and that the V_s modulation induced by the AC component of V_b has sufficient amplitude to use feedback control with lock-in detection. When the bias is fixed at a certain voltage except for V_{b0}, maps of lock-in output give $\partial(\Delta f)/\partial V_b$ images corresponding to capacitance images (figure 2(b) lower). These images indicate distribution of the electric-field-induced polarization caused by dielectric constant variations.

In all observations, electric potential images or surface capacitance images are obtained simultaneously with topography. These images were analyzed using the Win SPM Process (JEOL) and SPIP Metrology (Image Metrology) software packages.

3. Results and discussion

Topography and simultaneously obtained electric potential images of DNA and transcription complex are shown in figure 3. Figure 3(a) shows topography of string-like DNA and globular-shaped T7 RNA polymerase. This image comprises complex formation of T7 RNA polymerase with DNA because such globular-shaped protrusions were not observed in the control experiment quenching the transcription reaction (the experimental detail and AFM images are available in supporting materials available at stacks.iop.org/Nano/20/145102). Generally, T7 RNA polymerase binds at a specific region of DNA, and then advances along the DNA to synthesize mRNA, and finally separates from the DNA [13, 14]. To avoid this detachment, T7 RNA polymerase is anchored on a specific site of plasmid DNA using the reaction mixture without CTP, as described in the preparation of DNA and protein complex section. In fact, free T7 RNA polymerase cannot be seen in the image.

The electric potential image in figure 3(b) shows dark contrast for both DNA and T7 RNA polymerase complex. In this image, the dark region corresponds to the high V_{b0} indicating the area of low electric potential because V_{b0} bias compensates for the electric potential difference between the tip and the surface. Observed V_{b0} for DNA and T7 RNA polymerase bound on DNA are higher than -0.6 V for the mica surface clearly. The relationships between heights and V_{b0} values in various positions on the DNA and transcription complexes are shown in figure 4. The DNA heights observed in the topography are distributed into two ranges: from 1.0 to 1.4 nm for isolated DNA and from 1.6 to 2.0 nm for tangled DNA. The electric potential image showed different averaged

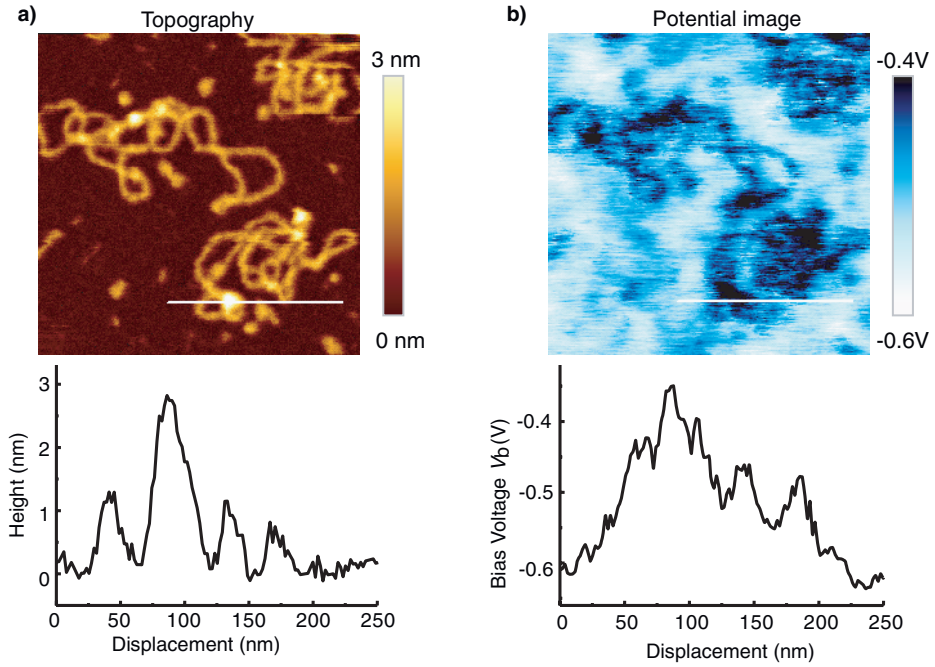

Figure 3. Electric potential image of DNA and transcription complexes. (a) Topography of DNA and transcription complex. Section profile showed that the heights of DNA and transcription complex were 1.4 and 2.8 nm, respectively. (b) Electric potential image obtained simultaneously with the topography. The grayscale is proportional to the negative V_{b0} value because the bias V_{b0} compensates for the electric potential difference between the tip and surface and the high V_{b0} region (dark contrast) in the images indicates the area of low electric potential. Observed V_{b0} values were −0.45 V and −0.35 V for DNA and transcription complex, respectively, as compared to −0.6 V for the mica surface.

values between these two classes of DNA: −0.48 V for isolated DNA and −0.37 V for tangled DNA. These results indicate that the accumulation of DNA on the surface induces an increase of electric potential. In contrast, T7 RNA polymerase complexes, which are taller than tangled DNA, did not show such a large potential reduction. Despite the high protrusion of 3.0 nm in topography, the observed V_{b0} values were −0.37 V, which were similar to those of tangled DNA.

As mentioned above, the applied surface potential V_{s0} was estimated to be approx. $1/10V_{b0}$ by the finite element calculation. It is well known that dipole moment density is given by $(V_{s0}^{mol} - V_{s0}^{mica})\,\varepsilon_0$, where $V_{s0}^{mol} - V_{s0}^{mica}$ is the potential difference on the molecules from on the mica and ε_0 is the permittivity of free space [15]. According to this relational expression, isolated DNA adsorbed on a mica substrate has a dipole moment density of 0.039 D nm^{-2}. Since DNA molecules adsorbed on the mica substrate preserve 3.4 nm periodicity of the B-form double helix [16], this dipole moment density corresponds to 0.027 D/base. Fundamentally, DNA should have no dipole moment along the transverse direction due to its coaxial structure. However, there is a possibility of generating an electric dipole induced by distortion. The height of DNA on the mica substrate is about 1.2 nm, which is smaller than the diameter of DNA in aqueous solution, and this low profile indicates a strongly-collapsed coaxial structure of DNA at the surface. The phosphate group at the top of DNA molecule spreads into free space, while that of the DNA–substrate interface is compressed strongly. This structural asymmetry induces electric dipoles whose positive ends face

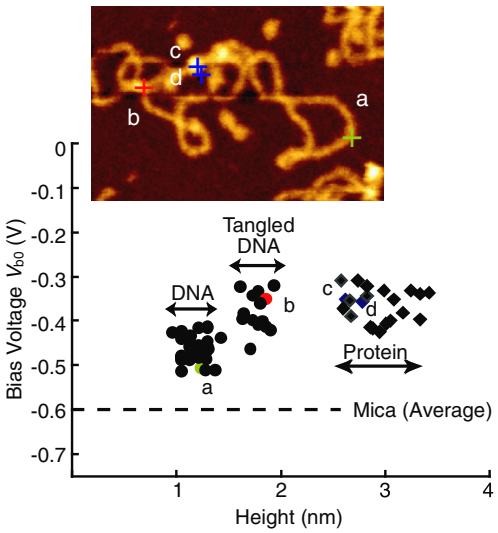

Figure 4. Height and electric potential distribution. The plots show three classes of height distribution: from 1.0 to 1.4 nm for isolated DNA, from 1.6 to 2.0 nm for tangled DNA and from 2.6 to 3.4 nm for transcription complex with V_b ranging from −0.52 to −0.40 V, from −0.42 to −0.31 V and from −0.41 to −0.3 V, respectively. The labels a–d in the topography (inset) correspond to the plots a–d indicating typical points in each category.

to the surface. Partial ionization of the phosphate groups with the surface water layer is also another possible mechanism to form an upward electric dipole (the positive end faces to the surface) on DNA molecules. In this case, counter cations

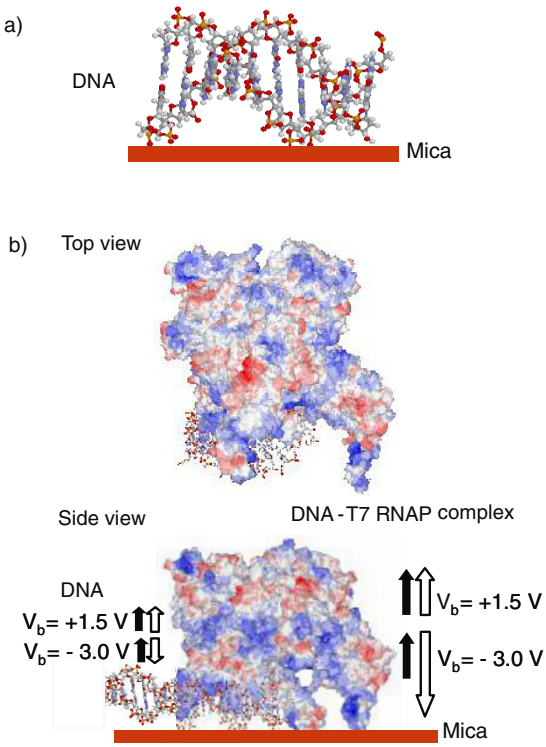

Figure 5. Schematic illustration of transcription complex. (a) DNA and (b) DNA and T7 RNA polymerase complex (Protein Data Bank accession number 1QLN). The model of T7 RNA polymerase is colored according to the electrostatic potential (positive, negative and neutral are blue, red and white, respectively) using MDL® Chime. DNA strands are shown as a ball-and-stick model. Field-induced polarization of T7 RNA polymerase is parallel and antiparallel at $V_b = 1.5$ and -3.0 V, respectively, to the permanent dipole.

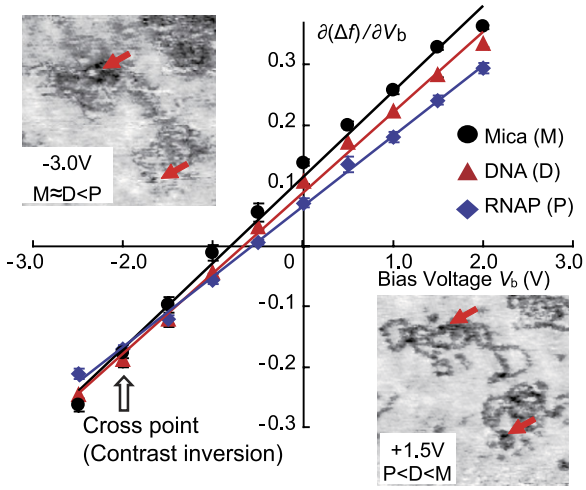

Figure 6. Capacitance images and $\partial(\Delta f)/\partial V_b$ versus V_b plots for DNA and DNA–RNA polymerase transcription complex on a mica substrate. The grayscale is proportional to the $\partial(\Delta f)/\partial V_b$ value and the dark contrast implies high polarizability. Arrows in the capacitance images indicate the positions of the transcription complexes. At $V_b = 1.5$ V, both DNA and the transcription complex were clearly observed with dark contrast against the mica surface. In contrast, at $V_b = -3.0$ V, DNA was obscured with dark contrast but the transcription complex had brightened. The plots of $\partial(\Delta f)/\partial V_b$ versus V_b show clearly that the crossing resulting contrast inversion around $V_b = -2.0$ V can be attributed to the differences in polarizability among the DNA, transcription complex and mica substrate.

of the phosphate groups diffuse into the water layer and the electric dipole arises around the phosphate groups due to local imbalance of positive and negative charge density.

Compared with DNA, T7 RNA polymerase has an intrinsic dipole moment, as shown in figure 5, where red and blue indicate negative and positive charge, respectively. The positive part of this protein binds with DNA to form a transcription complex. As a result, the positive end of the protein dipole faces to the surface (upward orientation). In this orientation, the dipoles of protein and DNA form head-to-tail alignment and partially cancel out their charges. Even then, in comparison with DNA alone, the total dipole density of the DNA/T7 RNA polymerase complex still shows a large value of 0.065 D nm^{-2} with upward orientation (the positive end faces to the surface). Since the electric charge is confined in the DNA/T7 RNA polymerase complex, the dipole can be expressed by molecular units, 0.16 D/molecule. As described later, the dipole is variable in response to an applied external field reflecting the flexible molecular structure. The dipole moment of the transcription complex was discussed in a previous report using capacitance measurements in solution [17]. This study is important as a complementary approach to our investigation. However, it is difficult to argue a comparative relation because the measurement provides overall and averaged dipole moments including molecular reorientation for a large number of transcription complexes with ionized state in solution. In fact, the reported value of dielectric constant ε is in the range of 60–80 and the values are one or two orders higher than the molecular dielectric constant.

Scanning capacitance microscopy probes electric-field-induced polarization of DNA and transcription complex. Figure 6 shows a $\partial(\Delta f)/\partial V_b$ image of DNA and transcription complex at bias voltages of $+1.5$ and -3.0 V applied to the electrode at the sample holder. As these voltages are very different from V_{b0}, capacitance ($\partial(\Delta f)/\partial V_b$) images exhibit field-induced electric properties. At $V_b = 1.5$ V, both DNA and the transcription complex were clearly observed with dark contrast against the mica surface. In contrast, at $V_b = -3.0$ V, DNA was obscured with dark contrast but the transcription complex had brightened. This contrast inversion implies crossing of $\partial(\Delta f)/\partial V_b$ versus V_b lines, as shown in figure 6. In these plots, the V_b-axis intersection of each line corresponds to the V_{b0} value and the slope indicates the dielectric constant. Although the absolute values of the electric potential and dielectric constant on an insulator substrate can be determined only by numerical calculation, the comparative measurement among target molecules and substrate is useful to examine electric properties of adsorbed nanostructures. The plots in figure 6 show clearly that the crossing resulting contrast inversion around $V_b = -2.0$ V can be attributed to the differences in polarizability among the DNA, transcription complex and mica substrate. These results suggest that the polarizability of the transcription complex is larger than that of DNA, indicating the large and flexible molecular structure of T7 RNA polymerase.

In summary, we demonstrated the utility of electrostatic force microscopy of biological molecules. The results open the possibility of studying the electrostatic properties of biological molecules and complexes on a one-by-one basis on commonly used insulator substrates with reduced inactivation. Using different responses to an external electric field, this method is potentially useful to discriminate biological molecules and complexes, such as small proteins, DNA oligomers and knotted-string-like tangled regions of DNA, which have similar topographic appearances.

Acknowledgments

This work was partially supported by a grant from the New Energy and Industrial Technology Development Organization (NEDO), Japan and a Grant-in-Aid for Scientific Research (KAKENHI), No. 20360020 from the Ministry of Education, Culture, Sports, Science an Technology (MEXT), Japan.

References

[1] Yodh J G, Lyubchenko Y L, Shlyakhtenko L S, Woodbury N and Lohr D 1999 Evidence for nonrandom behavior in 208–212 subsaturated nucleosomal array populations analyzed by AFM *Biochemistry* **38** 15756–63

[2] Rivetti C, Guthold M and Bustamante C 1999 Wrapping of DNA around the *E. coli* RNA polymerase open promoter complex *EMBO J.* **18** 4464–75

[3] Hansma H G, Oroudjev E, Baudrey S and Jaeger L 2003 TectoRNA and 'kissing-loop' RNA: atomic force microscopy of self-assembling RNA structures *J. Microsc.* **212** 273–9

[4] Abdelhady H G, Allen S, Davies M C, Roberts C J, Tendler S J and Williams P M 2003 Direct real-time molecular scale visualisation of the degradation of condensed DNA complexes exposed to DNase *Nucleic Acids Res.* **31** 4001–5

[5] Davies E, Teng K S, Conlan R S and Wilks S P 2005 Ultra-high resolution imaging of DNA and nucleosomes using non-contact atomic force microscopy *FEBS Lett.* **579** 1702–6

[6] Müller D J and Engel A 2007 Atomic force microscopy and spectroscopy of native membrane proteins *Nat. Protoc.* **2** 2191–7

[7] Mikamo E, Tanaka C, Kanno T, Akiyama H, Jung G, Tanaka H and Kawai T 2005 Native polysomes of *Saccharomyces cerevisiae* in liquid solution observed by atomic force microscopy *J. Struct. Biol.* **151** 106–10

[8] Pelling A E, Li Y, Shi W and Gimzewski J K 2005 Nanoscale visualization and characterization of *Myxococcus xanthus cells* with atomic force microscopy *Proc. Natl Acad. Sci. USA* **102** 6484–9

[9] Franz C M and Müller D J 2005 Analyzing focal adhesion structure by atomic force microscopy *J. Cell Sci.* **118** 5315–23

[10] Voïtchovsky K, Contera S A, Kamihira M, Watts A and Ryan J F 2006 Differential stiffness and lipid mobility in the leaflets of purple membranes *Biophys. J.* **90** 2075–85

[11] Lü J, Delamarche E, Eng L, Bennewitz R, Meyer E and Güntherodt H-J 1999 Kelvin probe force microscopy on surfaces: investigation of the surface potential of self-assembled monolayers on gold *Langmuir* **15** 8184–8

[12] Albrecht T R, Grtitter P, Horne D and Rugar D 1991 Frequency modulation detection using high-Q cantilevers for enhanced force microscope sensitivity *J. Appl. Phys.* **69** 668–73

[13] Henkin T M 1996 Control of transcription termination in prokaryotes *Annu. Rev. Genet.* **30** 35–57

[14] Rivetti C, Codeluppi S, Dieci G and Bustamante C 2003 Visualizing RNA extrusion and DNA wrapping in transcription elongation complexes of bacterial and eukaryotic RNA polymerases *J. Mol. Biol.* **326** 1413–26

[15] Weber R E and Peria W T 1969 Work function and structural studies of alkali-covered semiconductors *Surf. Sci.* **14** 13–38

[16] Maeda Y, Matsumoto T, Tanaka H and Kawai T 1999 Imaging of the DNA double helix structure by noncontact atomic force microscopy *Japan. J. Appl. Phys.* **38** L1211–2

[17] Choi C H, Sabourin N A, Reagor D W, Redondo A and Usheva A 2004 Capacitance-derived dielectric constants demonstrate differential preinitiation complexes in TBP-independent and TBP-dependent transcription *Biophys. Chem.* **111** 9–14